http://dx.doi.org/10.5012/bkcs.2014.35.8.2423

Template Synthesis of Nitrogen-Doped Short Tubular Carbons with Big Inner Diameter and their Application in Electrochemical Sensing

Rui Cheng,[a] Qiong Zou,[a] Xiaohua Zhang,[*] Chunhui Xiao, Longfei Sun, and Jinhua Chen[*]

State Key Laboratory of Chemo/Biosensing and Chemometrics, College of Chemistry and Chemical Engineering, Hunan University, Changsha 410082, P.R. China. [*]E-mail: chenjinhua@hnu.edu.cn (J. Chen); mickyxie@hnu.edu.cn (X. Zhang)
Received December 4, 2013, Accepted April 24, 2014

Nitrogen-doped short tubular carbons (N-STCs) with big inner diameter have been successfully synthesized *via* carbonization of polydopamine (PDA) wrapped halloysite nanotubes (HNTs). The obtained N-STCs have average length of 0.3 μm with big inner diameter (50 nm), thin wall (2-3 nm) and large surface area (776 $m^2 g^{-1}$), and show excellent electrochemical properties. As an example in electrochemical applications, N-STCs were used to electrochemically detect hydrogen peroxide (H_2O_2) and glucose. The results showed that the N-STCs modified glassy carbon (N-STCs/GC) electrode had much better analytical performance (lower detection limit and wider linear range) compared to the acid-treated carbon nanotubes (AO-CNTs) based GC electrode. The unique structure endows N-STCs the enhanced electrochemical performance and promising applications in electrochemical sensing.

Key Words : Nitrogen-doped short tubular carbons, Halloysite nanotubes, Electrochemistry, Template synthesis

Introduction

Various carbon materials, such as activated carbon, graphene, carbon fibres, carbon nanotubes, carbon aerogels and xerogels, have attracted a great deal of attention in electrochemical applications ranging from energy conversion and storage devices to sensitive sensors, due to their unique electrical and chemical properties.[1-3] Among them, one-dimensional (1D) carbon nanostructural materials, especially carbon nanotubes (CNTs), are of great fundamental and practical interests because of their high specific surface areas, fast kinetics, and short transport/diffusion path lengths for electrons and ions.[4] It has also been reported that the structure and morphology of CNTs affect the number of defective sites for reaction, electron transfer rate and mass transfer process, thus leading to considerably different performance in these applications.[5]

Recently, many efforts have been made to further improve the electrochemical properties of CNTs. For instance, to introduce more active sites, various kinds of surface functionalization methods, such as chemical or electrochemical oxidation at defect sites of CNTs,[6] heteroatoms doping[7] and wrapping of CNTs with polymer,[8] were generally carried out. On the other hand, to regulate the structural characteristics and morphologies of CNTs, some CNTs with special structure of thin carbon wall, small length scale, open ends or rich macro/mesopores have been developed.[9,10] It is believed that short nanotubes with open ends would create much more defects for reaction than the closed ones.[9-11] Meanwhile, the introduction of heteroatoms to carbon materials (such as nitrogen doping) not only yields a great deal of defective sites but changes the electron donor/acceptor characteristics of carbon materials, leading to great improvement in electrochemical performance and catalytic activity.[7,12-14] In addition, rich mesopores and/or macropores are also important for biomolecule and ion transfer in the reaction process on the carbon material surface.[15] Thus, the central pore of carbon nanotubes (the so-called inner diameter) could affect the mass transfer greatly. Many reports have demonstrated carbon tubes with big inner diameter could be readily filled with various liquids and suspensions, and facilitate the flow of biomolecules in the tubes.[16,17] However, the synthesis of typical CNTs with big inner diameter, rich mesopores on the wall of CNTs, short and open ends is still a challenge. Developing a simple method to prepare nitrogen-doped short tubular carbons (N-STCs) with above characteristics (big inner diameter, rich mesopores on the wall, short and open ends) for electrochemical applications is desirable.

Halloysite nanotubes (HNTs) is a type of natural occurring clay mineral comprised of siloxane groups (Si-O-Si) on the external surface, while gibbsite octahedral array (Al-OH) groups on the internal surface.[18] Taking HNTs as the template, N-STCs could be prepared by pyrolysis of polydopamine (PDA)[19,20] wrapped HNTs. The morphology, structure and electrochemical properties were characterized. Furthermore, as the examples in electrochemical applications, N-STCs were used to electrochemically detect hydrogen peroxide (H_2O_2) and glucose.

Experimental

Reagents and Materials. Dopamine hydrochloride (DA) was purchased from Alfa-Aesar and used as received. Multi-walled carbon nanotubes (CNTs, > 95%, diameter 20-40 nm, length 5-15 μm) were purchased from Shenzhen Nanotech Port Co. (Shenzhen, China) and treated with acids (conc.

[a]These authors contributed equally to this work.

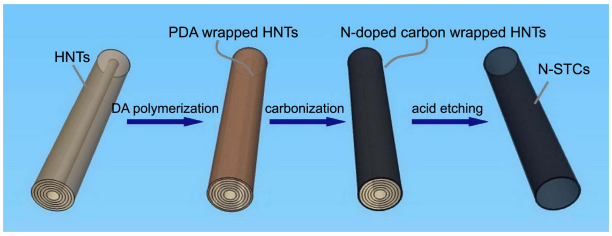

Scheme 1. Schematic diagram for preparation of N-STCs.

H_2SO_4 and conc. HNO_3, 3:1 V/V) (AO-CNTs) prior to use. HNTs were kindly donated by Zhengzhou Jinyangguang Chinaware Co. Ltd. (Henan, China) and purified by passing through 200-mesh sieve. Glucose oxidase (GOD) from Aspergillus niger (150,000 U g^{-1} solid) was purchased from Sigma-Aldrich. All other reagents were of analytical grade. Aqueous solutions used throughout were prepared with ultra pure water (> 18 MΩ cm) obtained from a Millipore system. Glucose stock solution was stored overnight at room temperature before use.

Synthesis of N-STCs. The preparation of N-STCs was composed of three steps (Scheme 1). In brief, HNTs (1000 mg) were washed thoroughly with tris(hydroxymethyl)-aminomethane (TRIS) buffer (50 mM, pH 8.5) and centrifuged three times. The deposit was resuspended in 400 mL TRIS buffer (50 mM, pH 8.5) containing DA (2 mg mL^{-1}), followed by vigorous stirring for 24 h to form PDA-wrapped HNTs (PDA/HNTs). The resulting dark green precipitates were centrifuged (3,000 rpm, 1 min) and washed with fresh TRIS buffer to remove the tan colored solution, followed by drying in vacuum at 60 °C overnight. Then, the nitrogen-doped carbon wrapped HNTs were obtained by carbonizing the PDA/HNTs in nitrogen atmosphere at 1000 °C for 2 h. Finally, N-STCs were obtained *via* removal of the template (HNTs core) in conc. HF for 15 h and then in conc. HCl for 6 h, followed by successive centrifugation (8,000 rpm, 5 min) and washing several times, and drying in vacuum at 60 °C overnight.

Characterization. The morphology of N-STCs was characterized by scanning electron microscopy (SEM, JSM 6700F, Japan) and transmission electron microscopy (TEM, JEM-2100F, Japan) equipped with an energy dispersive X-ray spectroscopy (EDS, GENESIS, EDAX, USA). Nitrogen adsorption-desorption isotherms and Brunauer-Emmett-Teller (BET) surface area were measured by an ASAP 2010 Micrometrics sorptometer (USA). Thermogravimetric analysis (TGA) was performed on a NETZSCH STA 409PC instrument at a heating rate of 5 °C min^{-1} under nitrogen gas flow. Nitrogen content in N-STCs was detected by an elemental analyzer (TCH-600, USA) and about 6.01 wt %. X-ray photoelectron spectra (XPS, Thermo Fisher Scientific K-Alpha 1063, UK) were recorded with an Al Kα X-ray source. For comparison, the morphology and porosity of AO-CNTs have also been investigated.

Electrochemical Evaluation. All electrochemical measurements were carried out on a CHI 660D electrochemical workstation (Chenhua Instrument Company of Shanghai, China) with a conventional three-electrode system comprising a platinum wire as the counter electrode, a saturated calomel electrode (SCE) as the reference electrode and modified glassy carbon (GC) electrode (3 mm in diameter) as the working electrode. All the potentials in this paper were referred to SCE and all electrochemical measurements were carried out at room temperature (25 ± 2 °C).

Prior to use, GC electrodes were polished with 0.3 and 0.05 μm alumina slurry sequentially to mirror-like electrodes, and then washed ultrasonically in water and ethanol for several minutes and dried with high-purity nitrogen stream.

The working electrode was prepared as follows: The obtained N-STCs (2 mg) were suspended in 1 mL ultrapure water to form N-STCs suspension with a concentration of 2 mg mL^{-1}. Then, 1 mL of N-STCs suspension (2 mg mL^{-1}) was mixed with 1 mL of EtOH and 10 μL of Nafion solution (5.0 wt %), and 6 μL of this mixture was coated onto the well-polished GC electrode to obtain the N-STCs modified GC (N-STCs/GC) electrode and dried in air at room temperature. For comparison, the AO-CNTs modified GC (AO-CNTs/GC) was prepared in the same way. For preparing enzyme electrode, 200 μL of N-STCs suspension (2 mg mL^{-1}) and 160 μL of GOD aqueous solution (10 mg mL^{-1}) was mixed for 5 min, then 40 μL of GA (50 wt %) was added with stirring, and the mixture was stored at 4 °C for 2 h. 6 μL of this mixture was coated onto the well-polished GC electrode to obtain the GOD/N-STCs modified GC (GOD/N-STCs/GC) electrode. The resulting enzyme electrode (GOD/N-STCs/GC electrode) was dried at 4 °C overnight and rinsed with ultrapure water before use. For comparison, the GOD/AO-CNTs/GC electrode was prepared in the same way.

Results and Discussion

Characterization of N-STCs. Figure 1 is the TGA results of pure HNTs (curve a) and PDA/HNTs (curve b). As shown in Figure 1, HNTs have an initial weight loss (less than 4.0 wt % below 416 °C) due to residual water and a major weight loss started at 416 °C which is assigned to the dehydroxylation of structural aluminol groups present in HNTs,[21] and remain comparably stable at higher temperature. The total weight loss of HNTs is *ca.* 15.0 wt % at 1000 °C (curve a). For PDA/HNTs, the weight loss is 26.6 wt % at 1000 °C (curve b). From the difference between the weight loss of the HNTs with and without PDA at 1000 °C, the amount of the PDA on HNTs was estimated to be about 11.6 wt %. The TGA results confirm that DA has undergone self-polymerization on the surface of HNTs.

The morphology, structure and elemental composition of the synthesized N-STCs were characterized by SEM, TEM and EDS, respectively. The SEM and TEM images of N-STCs reveals the formation of uniform tubular carbon microstructures with short length and big inner diameter of about 0.3 μm and 50 nm, respectively, as illustrated in Figures 2(a) and 2(b). It is noteworthy that the tubes with open ends look almost transparent, indicating that the wall

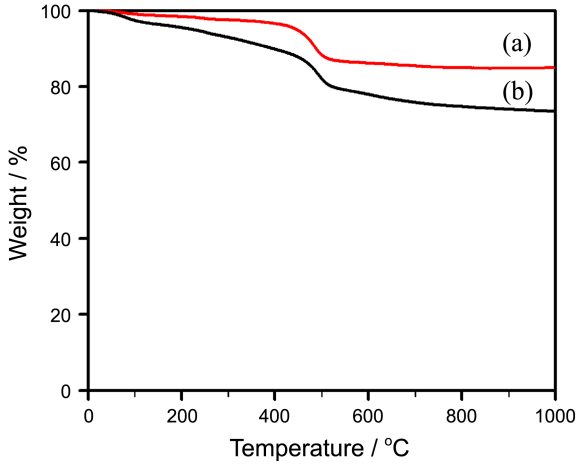

Figure 1. The TGA results of HNTs (a) and PDA/HNTs (b).

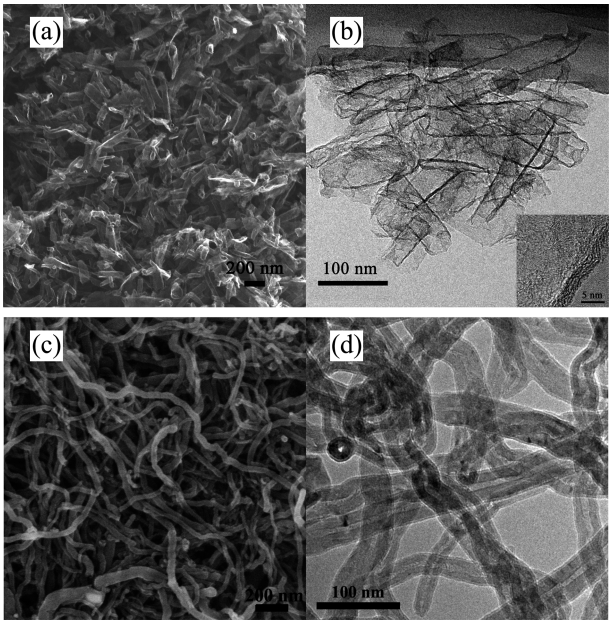

Figure 2. SEM and TEM images of N-STCs (a, b) and AO-CNTs (c, d). The inset in Figure 2(b), the HRTEM image of N-STCs.

thickness of the tubes is very thin.[22] This was further confirmed in the high-resolution TEM image. From the inset image in Figure 2(b), it can be observed that the wall thickness of N-STCs is only 2-3 nm and is thinner than that of many reported carbon nanotubes.[9,15] For comparison, the morphology of AO-CNTs was also investigated by SEM and TEM (Figs. 2(c) and 2(d)). It is noted that the inner diameter of AO-CNTs is about 5 nm (Fig. 2(c)), much smaller than that of N-STCs. However, the length (5–15 μm) of AO-CNTs is much longer than that of N-STCs. The structural features of N-STCs, such as short length, big inner diameter, open ends and thin wall, would render easy access, filling and transportation of foreign molecules. The EDS spectra (Fig. 3(a)) shows that C, N, O and Cu are the major elements in N-STCs, where Cu comes from the Cu foil, indicating the complete removal of the HNT template.

In order to clarify the structure of N atoms in N-STCs,

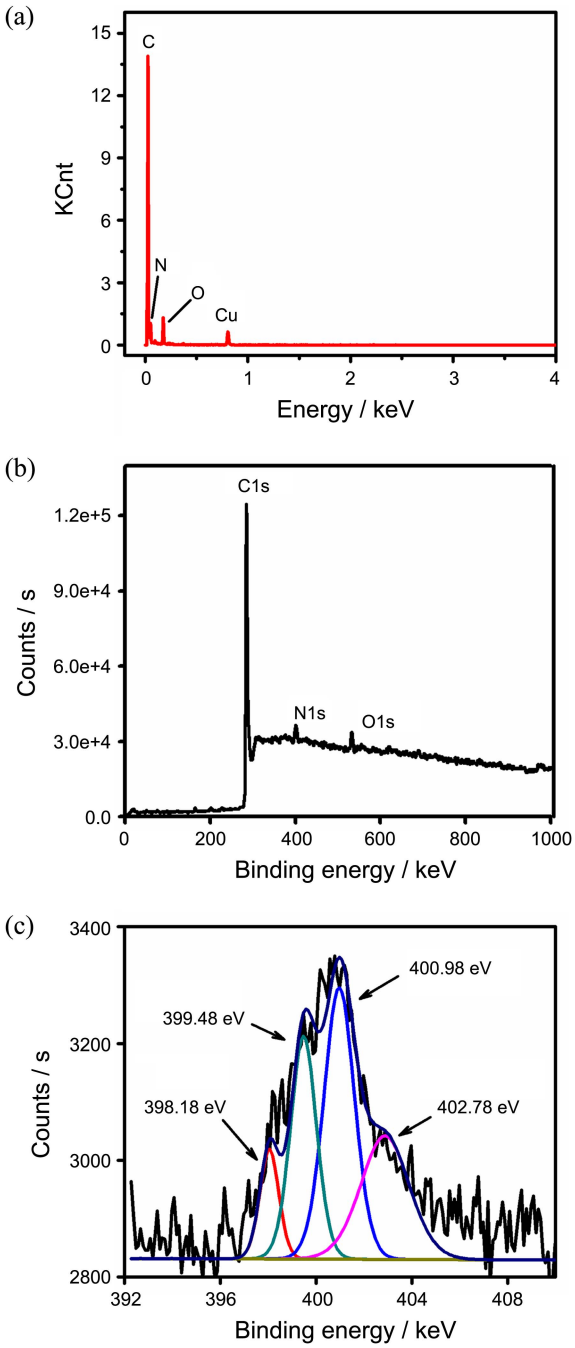

Figure 3. The EDS pattern (a), XPS wide angle spectrum (b) and high-resolution N 1s spectra (c) of N-STCs.

XPS characterization were further performed. The related XPS wide angle spectrum and high-resolution N 1s spectra for N-STCs are shown in Figures 3(b) and 3(c), respectively. Figure 3(b) confirms clearly the N doping of N-STCs. The bonding configuration of the nitrogen atoms in the N-STCs were further characterized by a high-resolution N1s spectrum. The N1s spectrum can be fitted into four peaks at 398.2, 399.5, 401.0, 402.8 eV (Fig. 3(c)). The peaks with lower binding energy located at about 398.2 and 399.5 eV correspond to pyridine-like and pyrrole-like nitrogen, respectively. When carbon atoms in N-STCs are substituted by

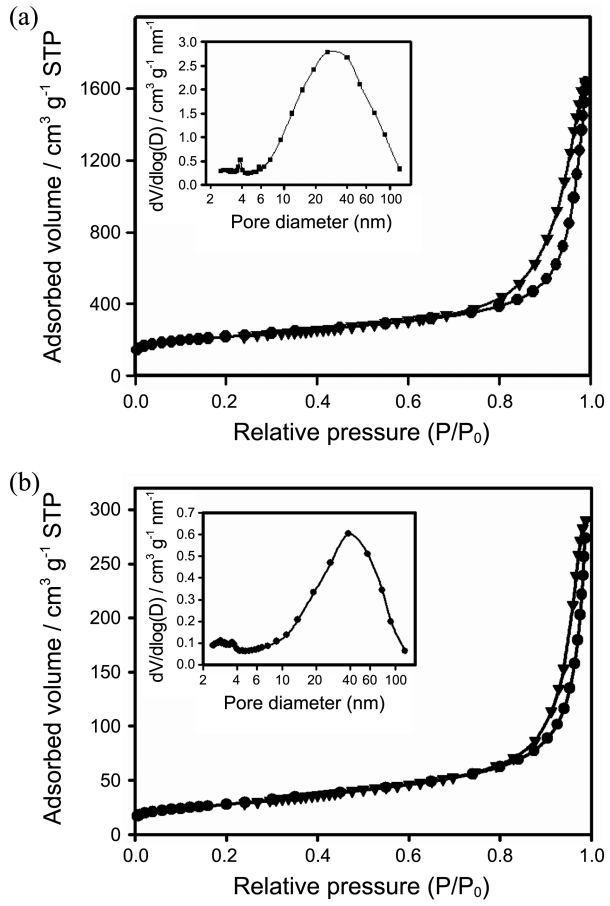

Figure 4. Nitrogen adsorption-desorption isotherms and the pore size distribution (the inset plot) of N-STCs (a) and AO-CNTs (b).

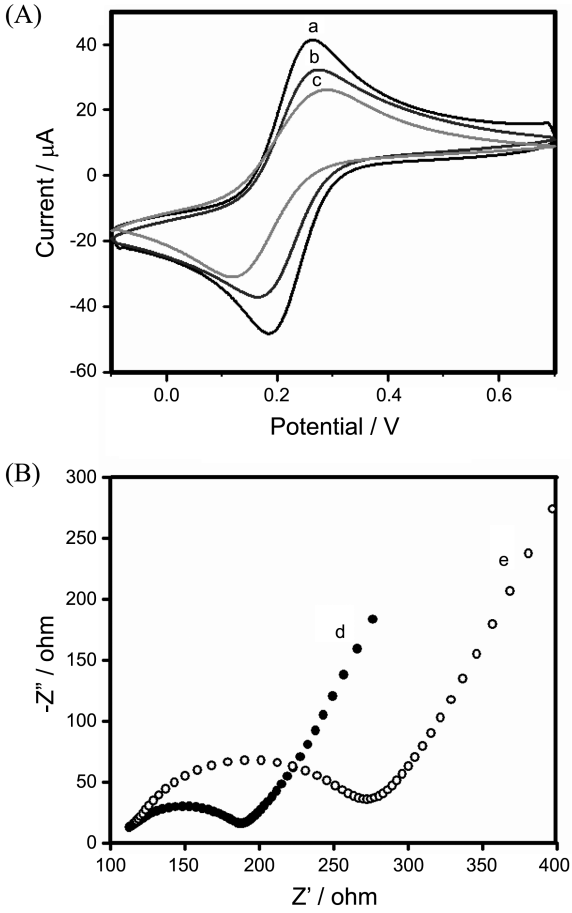

Figure 5. (A) Cyclic voltammograms obtained at N-STCs/GC (a), AO-CNTs/GC (b) and bare GC (c) electrodes in 5 mM $Fe(CN)_6^{3-/4-}$ (1:1) + 0.1 M KCl aqueous solution. Scan rate, 50 mV s^{-1}. (B) Electrochemical impedance spectroscopy (EIS) results obtained at N-STCs/GC (d) and AO-CNTs/GC (e) electrodes in 5 mM $Fe(CN)_6^{3-/4-}$ (1:1) + 0.1 M KCl aqueous solution.

nitrogen atoms in the form of "graphitic" nitrogen, the corresponding peak in the N1s spectrum is located at 400.8-401.3 eV. The peak at 402.8 eV is attributed to oxidized nitrogen.[23] The N1s spectrum shows that "graphitic" nitrogen is the main component in N-STCs, which may improve the electrocatalytic activity of N-STCs.[24,25]

For further understanding the porous texture, N_2 adsorption-desorption isotherms of N-STCs were measured. The corresponding N_2 adsorption-desorption isotherms and pore size distribution are shown in Figure 4. From Figure 4(a), the isotherms of N-STCs show a type IV isotherm and type H1 hysteresis loops,[15] indicating the presence of a high proportion of mesopores.[15,26] To obtain more detail information on the porosity, the pore size distribution (PSD) was calculated *via* the BJH model (the inset plot in Fig. 4(a)). The pore size distribution has two clear peaks corresponding to a narrow distribution centered at around 4 nm and a much broader distribution around 30 nm, which correspond to small mesopores in the wall of N-STCs and large mesopores resulting from the tube spaces and spaces between the close-packed N-STCs, respectively.[15,27] Although the isotherms and the pore size distribution of AO-CNTs (Fig. 4(b)) are similar with that of N-STCs, the BET specific surface area and the pore volume of N-STCs (776 m^2 g^{-1}, 2.47 cm^3 g^{-1}) are much larger than those of AO-CNTs (119.4 m^2 g^{-1}, 0.40 cm^3 g^{-1}), which should result from the structural feature of N-STCs (short length, big inner diameter and open ends).

With rich mesopores, large surface area, special tubular structure and nitrogen doping, N-STCs is expected to have good electrochemical properties and could be a desirable electrode material for advanced sensors and highly efficient energy storage and conversion devices.[3,14]

Electrochemical Properties of N-STCs. $Fe(CN_6)^{3-/4-}$ is widely used as an electrochemical probe to evaluate the electrochemical properties of the electrode. The cyclic voltammograms of the N-STCs/GC (curve a), AO-CNTs/GC (curve b), and bare GC (curve c) electrodes in $Fe(CN_6)^{3-/4-}$ (5 mM $Fe(CN_6)^{3-/4-}$ + 0.1 M KCl) solution are shown in Figure 5(A). The peak potential separation (ΔE_p) at the N-STCs/GC electrode is 72 mV, while the ΔE_p at the AO-CNTs/GC and bare GC electrodes are 103 mV and 166 mV, respectively, indicating that the N-STCs/GC electrode has higher electron transfer rate compared with the AO-CNTs/GC and bare GC electrodes.[28] Moreover, the N-STCs/GC electrode displays much higher redox peak currents than those of the AO-CNTs/GC and bare GC electrodes. Both the

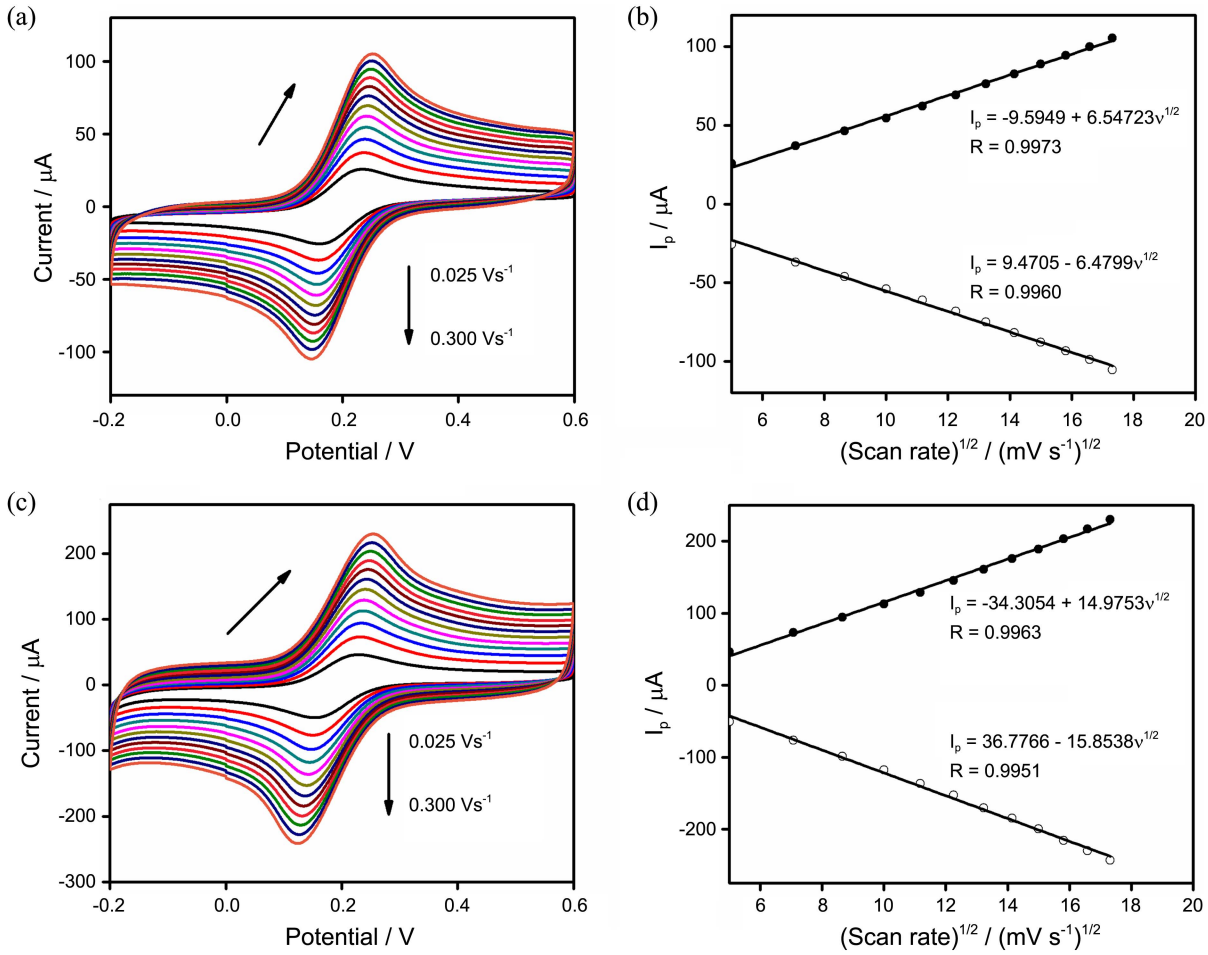

Figure 6. Cyclic voltammograms obtained at the AO-CNTs/GC (a) and N-STCs/GC (c) electrodes in 5 mM $Fe(CN)_6^{3-/4-}$ (1:1) + 0.1 M KCl aqueous solution at different scan rate (from inner to outer, 0.025, 0.050, 0.075, 0.100, 0.125, 0.150, 0.175, 0.200, 0.225, 0.250, 0.275, 0.300 V s^{-1}). The dependence of the anodic and cathodic peak currents obtained at the AO-CNTs/GC (b) and N-STCs/GC (d) electrodes on the square root of scan rate.

smaller ΔE_p and the higher redox peak currents would imply the better electrochemical performance of N-STCs/GC electrode.

On the other hand, the capability of electron transfer of different electrodes was also investigated by electrochemical impedance analysis shown in Figure 5(B). It is noted that the value of charge transfer resistance (R_{ct}) of the N-STCs/GC (curve d) electrode is smaller than that of the AO-CNTs/GC (curve e). This result is in accordance with that observed in Figure 5(A). Meanwhile, it re-conforms that N-STCs possess good conductivity and electrochemical properties. This may mainly be due to the more active edge sites of N-STCs resulting from N-doping.[29] In other words, N-STCs may be the promising active materials to construct electrochemical sensors.

Figure 6 shows the cyclic voltammograms of $Fe(CN_6)^{3-/4-}$ probe on the N-STCs/GC and AO-CNTs/GC electrodes at different scan rates and the corresponding oxidation and reduction peak currents as the function of the scan rate. It is noted that both oxidation and reduction peak currents of $Fe(CN_6)^{3-/4-}$ probe are linear with the square root of scan rates on both N-STCs/GC and AO-CNTs/GC electrodes. This implies that the redox performance of $Fe(CN_6)^{3-/4-}$ probe on both N-STCs/GC and AO-CNTs/GC electrodes is controlled by diffusion process. On the other hand, the linear slop in Figure 6(d) is much larger than that in Figure 6(b), indicating that N-STCs possess better mass transfer efficiency due to the unique structure (short length, big inner diameter and open ends) of N-STCs.

To further explore the applications of N-STCs in electrochemical fields, especially electrochemical sensing, the N-STCs modified electrodes were used to electrochemically detect hydrogen peroxide (H_2O_2) and glucose. H_2O_2 is not only an essential mediator in food, pharmaceutical, clinical, industrial, and environmental analyses, but also the product of enzymatic reactions between oxidase and their substrates.[30] Thus, the accurate determination of H_2O_2 is of great importance. Figure 7 shows the cyclic voltammograms of different electrodes in the absence and presence of 5 mM H_2O_2 in PBS solution (0.1 M, pH 7.0). To get rid of the interference of oxygen, the experiments were performed in nitrogen-saturated solution. As shown in Figure 7, when 5 mM H_2O_2 was added, the oxidation of H_2O_2 at the N-STCs/GC electrode starts at 0.16 V which is more negative than the onset

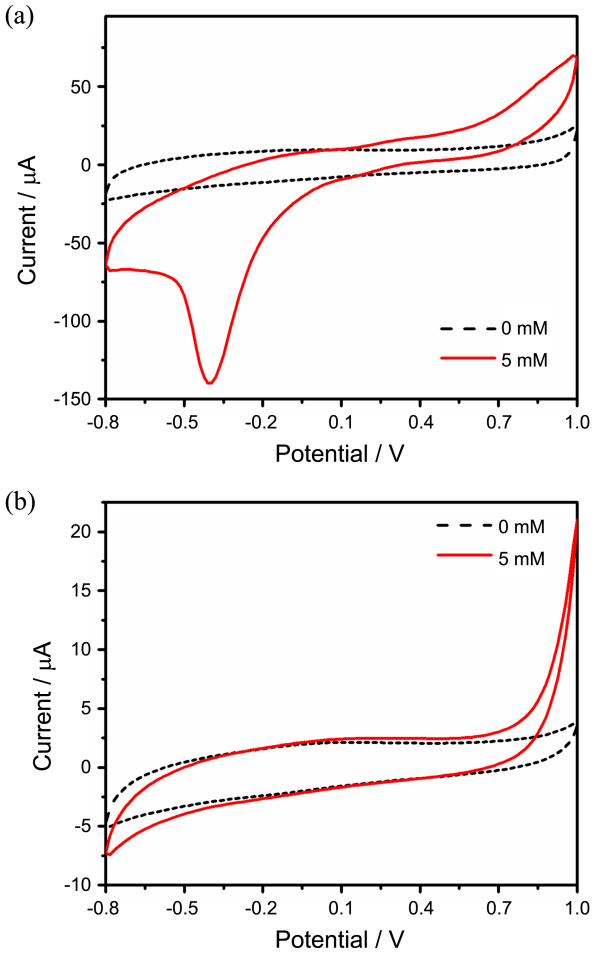

Figure 7. Cyclic voltammograms obtained at the N-STCs/GC (a) and AO-CNTs/GC (b) electrodes in nitrogen-saturated PBS (0.1 M, pH 7.0) with and without 5 mM H_2O_2 at the scan rate of 50 mV s^{-1}.

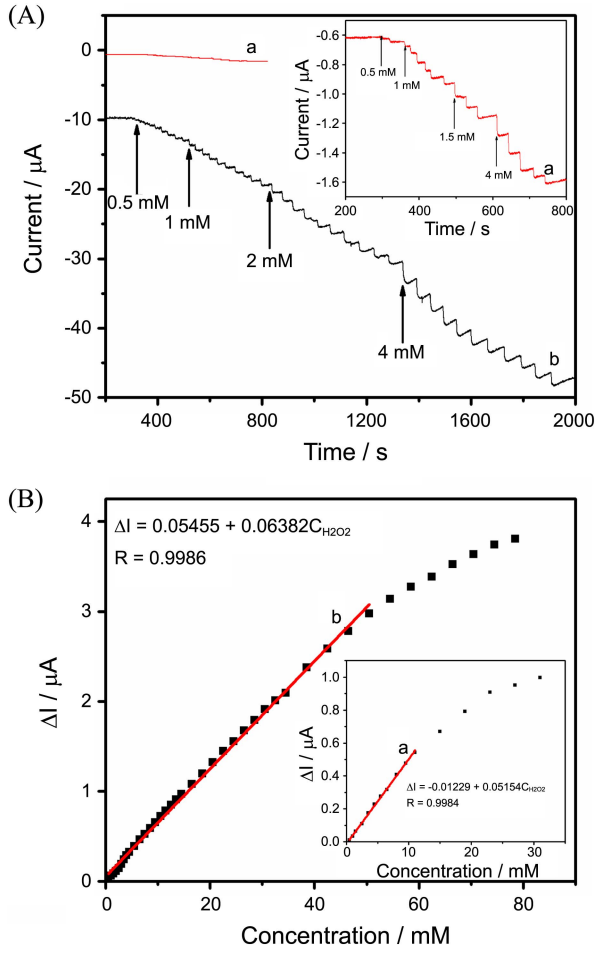

Figure 8. (A) Current responses obtained at the AO-CNTs/GC (a) and N-STCs/GC (b) electrodes to the successive addition of different concentrations of H_2O_2 in nitrogen-saturated PBS solution (0.1 M, pH 7.0), applied potential, at −0.2 V. The insert in Figure 8(A) is the enlarged plot of curve a. (B) The related calibration curves obtained at the AO-CNTs/GC (a) and N-STCs/GC (b). ΔI is the result of the initial current minus the steady-state current.

potential of H_2O_2 oxidation at the AO-CNTs/GC electrode (0.43 V). On the other hand, the onset potential of the reduction of H_2O_2 at the N-STCs/GC electrode is 0.14 V which is more positive than that at the AO-CNTs/GC electrode (−0.12 V). Furthermore, the H_2O_2 redox currents at the N-STCs/GC electrode are much higher than those at the AO-CNTs/GC electrode. These results suggest the superior electrocatalytic activity of N-STCs towards H_2O_2 oxidation and reduction. Furthermore, the amperometric responses of the N-STCs/GC and AO-CNTs/GC electrodes to the addition of hydrogen peroxide in 0.1 M PBS (pH 7.0) at an applied potential of −0.2 V are also shown in Figure 8. It is noted that the response currents at the AO-CNTs/GC electrode (Fig. 8(A), curve a or insert plot in Fig. 8(A)) are much smaller than that at the N-STCs/GC electrode (Fig. 8(A), curve b). From the calibration curves shown in Figure 8(B), it can be obtained that the linear response ranges at the N-STCs/GC and AO-CNTs/GC electrodes are up to 50.5 and 11.0 mM with the detection limits (S/N=3) of 0.26 and 0.38 mM, respectively. It is noted that that the linear range obtained on the N-STCs/GC electrode is much wider than that on the AO-CNTs/GC electrode, which should be contributed to the unique structure of N-STCs (short length, big inner diameter and open ends).

In addition, GOD, widely used in glucose monitoring, is taken as a model enzyme to further investigate the biosensing application of N-STCs. Figure 9(A) presents the cyclic voltammograms of different electrodes in nitrogen-saturated PBS (0.1 M, pH 7.0) at 50 mV s^{-1}. A pair of well-defined and quasi-reversible redox peaks corresponding to the direct electrochemistry of GOD are observed at both GOD/N-STCs/GC (curve a) and GOD/AO-CNTs/GC (curve b) electrodes, while the GOD/GC electrode does not show the redox peaks. The formal potential (E^0) of the GOD/N-STCs/GC and the GOD/AO-CNTs/GC electrodes are *ca.* −0.46 V and *ca.* −0.47 V, which are very close to the value reported previously.[31,32] On the other hand, the peak currents of curve a are larger than those of curve b. This demonstrates that the GOD/N-STCs/GC electrode is more beneficial to the direct electrochemistry of GOD than the GOD/AO-CNTs/GC electrode due to the same GOD amounts immobilized on both electrodes. Furthermore, from Figure 9(B), the anodic

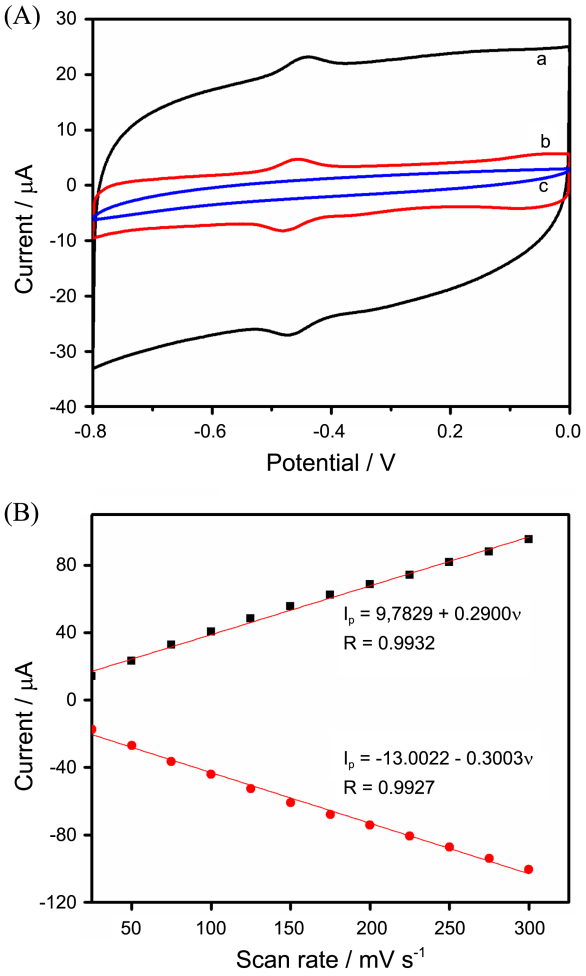

Figure 9. (A) Cyclic voltammograms obtained at the GOD/N-STCs/GC (a), GOD/AO-CNTs/GC (b), and GOD/GC (c) electrodes in nitrogen-saturated PBS (0.1 M, pH 7.0) at the scan rate of 50 mV s^{-1}. (B) The dependence of the anodic and cathodic peak currents of the GOD/N-STCs/GC electrode on the scan rates in nitrogen-saturated PBS (0.1 M, pH 7.0).

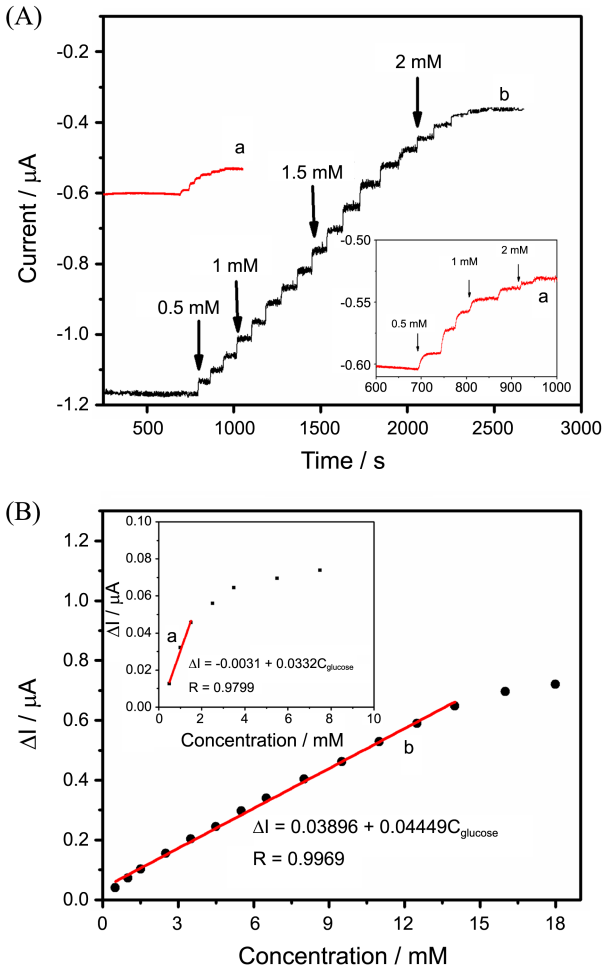

Figure 10. (A) Current responses obtained at the GOD/AO-CNTs/GC (a) and GOD/N-STCs/GC (b) electrodes to the successive addition of different concentrations of glucose in air-saturated PBS solution (0.1 M, pH 7.0), applied potential, at –0.46 V. The insert in Figure 10(A) is the enlarged plot of curve a. (B) The related calibration curves obtained at the GOD/AO-CNTs/GC (a) and GOD/N-STCs/GC (b). ΔI is the result of the steady-state current minus the initial current.

and cathodic peak currents increase linearly with the increase of the scan rate (from 25 to 300 mV s^{-1}), indicating that the electrochemical reaction of GOD immobilized on the N-STCs/GC electrode is a surface controlled process.[32]

In order to explore the applications of N-STCs in electrochemical biosensing of glucose based on the direct electrochemistry of GOD, the amperometric responses of the N-STCs/GC and AO-CNTs/GC electrodes to the addition of glucose have been investigated and the corresponding results are shown in Figure 10(A). It is noted that the response currents at the AO-CNTs/GC electrode (Fig. 10(A), curve a or the insert plot in Fig. 10(A)) are much smaller than that at the N-STCs/GC electrode (Fig. 10(A), curve b). From the calibration curves shown in Figure 10(B), it can be obtained that the linear response ranges at the N-STCs/GC and AO-CNTs/GC electrodes are up to 14.0 and 1.5 mM with the detection limits (S/N=3) of 0.29 and 0.36 mM, respectively. This indicates that N-STCs have better analytical performance than AO-CNTs in glucose biosensing, further suggesting that N-STCs may be an advanced material in electrochemical biosensors.

Conclusions

N-STCs with large surface area, rich mesopores, big inner diameter and open ends have been successfully prepared *via* pyrolysis of PDA wrapped halloysite nanotubes, and further investigated the potential applications in H_2O_2 redox reactions and glucose biosensor based on the direct electrochemistry of GOD. It was found that the electrochemical redox behavior of H_2O_2 and GOD has been greatly improved at the N-STCs/GC electrode due to the unique structure of N-STCs. Furthermore, compared with the AO-CNTs, the developed N-STCs show much better analytical performance (lower detection limit and wider linear range) for H_2O_2 and glucose detection. These indicate a great promising of N-STCs in electrochemical sensing. In addition, due to the

great surface area, special porous structure with big inner diameter and open ends, and nitrogen-doping, N-STCs could be also expected as useful support materials for energy storage and conversion devices such as supercapacitor and fuel cells, *etc.*

Acknowledgments. Publication cost of this article was supported by the Korean Chemical Society.

References

1. Zhang, L. L.; Zhao, X. *Chem. Soc. Rev.* **2009**, *38*, 2520.
2. Frackowiak, E.; Beguin, F. *Carbon* **2001**, *39*, 937.
3. Liang, C.; Li, Z.; Dai, S. *Angew. Chem. Int. Ed.* **2008**, *47*, 3696.
4. Baughman, R. H.; Zakhidov, A. A.; de Heer, W. A. *Science* **2002**, *297*, 787.
5. Yang, W.; Ratinac, K. R.; Ringer, S. P.; Thordarson, P.; Gooding, J. J.; Braet, F. *Angew. Chem. Int. Ed.* **2010**, *49*, 2114.
6. Chen, J.; Wang, M.; Liu, B.; Fan, Z.; Cui, K.; Kuang, Y. *J. Phy. Chem. B* **2006**, *110*, 11775.
7. Gong, K.; Du, F.; Xia, Z.; Durstock, M.; Dai, L. *Science* **2009**, *323*, 760.
8. Wu, B.; Hu, D.; Kuang, Y.; Liu, B.; Zhang, X.; Chen, J. *Angew. Chem. Int. Ed.* **2009**, *48*, 4751.
9. Hou, P.-X.; Yu, W.-J.; Shi, C.; Zhang, L.-L.; Liu, C.; Tian, X.-J.; Dong, Z.-L.; Cheng, H.-M. *J. Mater. Chem.* **2012**, *22*, 15221.
10. Pierard, N.; Fonseca, A.; Konya, Z.; Willems, I.; Tendeloo, G. V.; Nagy, J. B. *Chem. Phys. Lett.* **2001**, *335*, 1.
11. Pan, X.; Fan, Z.; Chen, W.; Ding, Y.; Luo, H.; Bao, X. *Nature Materials* **2007**, *6*, 507.
12. Yang, Q.; Xu, W.; Tomita, A.; Kyotani, T. *J. Am. Chem. Soc.* **2005**, *127*, 8956.
13. Jafri, R. I.; Rajalakshmi, N.; Ramaprabhu, S. *J. Mater. Chem.* **2010**, *20*, 7114.
14. Xiao, K.; Liu, Y.; Ping'an H.; Yu, G.; Sun, Y.; Zhu, D. *J. Am. Chem. Soc.* **2005**, *127*, 8614.
15. Jiang, H.; Zhao, T.; Li, C.; Ma, J. *Chem. Commun.* **2011**, *47*, 8590.
16. Whitby, M.; Quirke, N. *Nature Nanotechnology* **2007**, *2*, 87.
17. Kim, B.; Murray, T.; Bau, H. *Nanotechnology* **2005**, *16*, 1317.
18. Yah, W. O.; Takahara, A.; Lvov, Y. M. *J. Am. Chem. Soc.* **2012**, *134*, 1853.
19. Lee, H.; Dellatore, S. M.; Miller, W. M.; Messersmith, P. B. *Science* **2007**, *318*, 426.
20. Xiao, C.; Chu, X.; Yang, Y.; Li, X.; Zhang, X.; Chen, J. *Biosens. Bioelectron* **2011**, *26*, 2934.
21. Chang, P. R.; Xie, Y.; Wu, D.; Ma, X. *Carbohydr. Polym.* **2011**, *84*, 1426.
22. Kyotani, T.; Tsai, L.-F.; Tomita, A. *Chem. Mater.* **1995**, *7*, 1427.
23. Xu, F.; Minniti, M.; Barone, P.; Sindona, A.; Bonanno, A.; Oliva, A. *Carbon* **2008**, *46*, 1489.
24. Lai, L.; Potts, J. R.; Zhan, D.; Wang, L.; Poh, C. K.; Tang, C.; Gong, H.; Shen, Z.; Lin, J.; Ruoff, R. S. *Energy Environ. Sci.* **2012**, *5*, 7936.
25. Sharifi, T.; Hu, G.; Jia, X.; Wågberg, T. *ACS Nano* **2012**, *6*, 8904.
26. Lei, Z.; Zhao, M.; Dang, L.; An, L.; Lu, M.; Lo, A.-Y.; Yu, N.; Liu, S.-B. *J. Mater. Chem.* **2009**, *19*, 5985.
27. Zhang, H.; Cao, G.; Wang, Z.; Yang, Y.; Shi, Z.; Gu, Z.; *Electrochem. Commun.* **2008**, *10*, 1056.
28. Nicholson, R. S. *Anal. Chem.* **1965**, *37*, 1351.
29. Jia, N.; Wang, L.; Liu, L.; Zhou, Q.; Jiang, Z. *Electrochem. Commun.* **2005**, *7*, 349.
30. Veal, E. A.; Day, A. M.; Morgan, B. A. *Molecular Cell* **2007**, *26*, 1.
31. Wang, J. *Chem. Rev.* **2008**, *108*, 814.
32. Wu, S.; Ju, H.; Liu, Y. *Adv. Funct. Mater.* **2007**, *17*, 585.